Characterization of Deformability of Spheroidal Cementite by Residual Stress Measurement

Lei Che, Masahide Gotoh, Yoshiaki Horimoto, Yukio Hirose, and Lin Yang

This article deals with the characterization of the mechanical behaviors of spheroidized carbon steels, which contain ferrite and spheroidal cementite. The aim of the study is to identify the deformation behaviors of cementite particles by x-ray diffraction and to correlate them to the residual stress state evolution. The stress state evolutions for both phases during an *in situ* 4-point bending test and after a uniaxial tensile test that have been well followed by x-ray diffraction. After each tensile loading, optical observation is made to correlate the determined residual stress state with the microstructure. The coupling of techniques helps us to characterize the deformation evolution of spheroidal cementite in the carbon steel: at the initial state, the cementite shows the same elastic behavior as the ferrite; at the next state, the ferrite begins to deform plastically but the cementite deforms elastically; then, plastic relaxation occurs in the ferrite while the cementite still deforms elastically until finally breaking.

1. Introduction

Cementite is one of the most important constituents in carbon steels and is usually present in the forms of cementite lamellae in pearlite and spheriodite distributed in ferrite. Even though the cementite in carbon steels occupies less than one-fifth of their volume, the deformation and strength of such steels are profoundly affected by its presence. Previous studies have indicated that the strength of pearlite is proportional to the reciprocal square root of the average interlamellar spacing, and the proportionality constant is related to the strength of the cementite lamellae (Ref 1, 2). Our previous study has exhibited that the strength of spheroidized steel depends strongly both on cementite's volume fraction and it's particle size (Ref 3). Nevertheless, the cementite in carbon steels show a complicated deformability because of its dependence on temperature and microstructural morphology. For the plastically deformed pearlite steels, it has been recognized that there is an effect of thickness of the cementite plates on their deformability: the plasticity of cementite is obtained in fine pearlite from drawn or swaged wires, while brittleness of cementite is obtained in coarse pearlite from tension or compressing specimens (Ref 2, 4). Dissolution in cementite particles has also been observed in

the high-deformed pearlite and spheriodized steel (Ref 5, 6). In these studies, the deformation activities of the cementite are usually discussed by studying the changes in the dislocation sub-structure of cementite plates using optical techniques, such as scanning electron microscopy (SEM) and transmitting electron microscopy (TEM).

For a better understanding of the material mechanical response under loading, x-ray diffraction technique is used in this study to measure the stress states for the ferrite and the cementite separately. In order to well understand the deformation behaviors of ferrite and the cementite in steels, the misfit of plastic strain between the two phases in the deformation processing is estimated indirectly by x-ray measurement. Associating with optical observations, the deformability of the spheroidal cementite particle in the plastically deformed steel is characterized by the residual stress state evolution.

2. Theory

2.1 X-ray Measurement of Misfit of Plastic Strain in Two-phase Composite Material

For the dispersed two-phase material, in which one phase is the dispersed particle and is completely surrounded by the homogenous isotropic matrix, if it is subjected to uniaxial tensile stress, macro- as well as micro stresses are caused on a macroscopic and microscopic scale due to the different physical and mechanical properties of them as shown in Fig. 1. X-ray diffraction technique, as a nondestructive measurement method, is generally applied on estimating the internal stress state for each phase separately. We set up the coordinate system as shown in Fig. 2. σ_x is the stress in φ direction and ψ is the angle between the normal of diffraction plane and the normal of specimen surface. Based on this coordinate system, the relation between strains and stresses can be described as Eq 1.

Lei Che and **Yoshiaki Horimoto**, Graduate School, Kanazawa University, Kanazawa 920-1192, Japan; **Masahide Gotoh** and **Yukio Hirose**, Department of Risk Base System Engineering, Kanazawa University, Kanazawa 920-1192, Japan; and **Lin Yang**, School of Mechanical Engineering and Automation, Dalian Polytechnic University, Dalian 116034, China. Contact e-mail: che@cs.s.kanazawa-u.ac.jp.
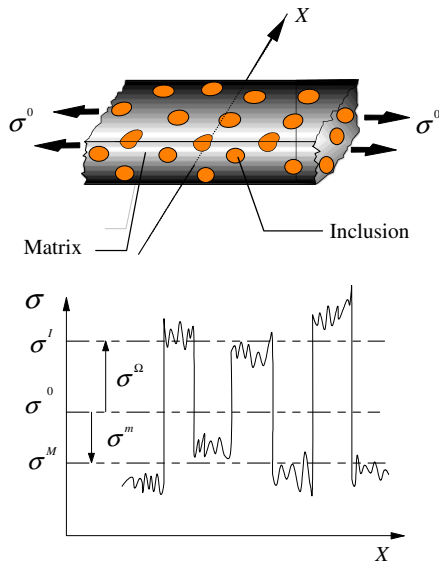
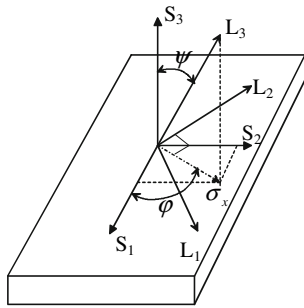**Fig. 1** Stresses in the two-phase composite material

Fig. 2 Coordinates of x-ray stress measurement

$$\varepsilon_{33}^{L} = \frac{S_2}{2}\left(\sigma_{11}\cos^2\varphi + \sigma_{12}\sin 2\varphi + \sigma_{22}\sin^2\varphi\right)\sin^2\psi$$
$$+ \frac{S_2}{2}\sigma_{33}\cos^2\psi + S_1(\sigma_{11} + \sigma_{22} + \sigma_{33})$$
$$+ \frac{S_2}{2}(\sigma_{13}\cos\varphi + \sigma_{23}\sin\varphi)\sin 2\psi$$

$$\text{(Eq 1)}$$

If only principal stresses σ_{11}, σ_{22}, and σ_{33} exist in the material, we make $\varphi = 0$, combined with Bragg's law, the following $2\theta_\psi - \sin^2\psi$ relation is obtained:

$$2\theta_\psi = -2\tan\theta_0\left\{\frac{S_2}{2}(\sigma_{11} - \sigma_{33})\sin^2\psi + \frac{S_2}{2}\sigma_{33}\right.$$
$$\left. + S_1(\sigma_{11} + \sigma_{22} + \sigma_{33})\right\} + 2\theta_0 \quad \text{(Eq 2)}$$

where, $2\theta_\psi$ is the diffraction angle; $2\theta_0$ refers to the diffraction angle of the material in free strain state; S_1 and S_2 are named as x-ray elastic constants (XEC), and can be given by:

$$S_1 = -\frac{\nu_x}{E_x}, \quad S_2 = \frac{2(1 + \nu_x)}{E_x} \quad \text{(Eq 3)}$$

E_x and ν_x are x-ray Young's modulus and Poisson's ratio, respectively.

Differentiating Eq 2 for $\sin^2\psi$, we obtain $\sigma_{11} - \sigma_{33}$ as follows:

$$\sigma_{11} - \sigma_{33} = -\frac{1}{S_2}\cdot\cot\theta_0\cdot\frac{\partial(2\theta_0)}{\partial(\sin^2\psi)}\cdot\frac{\pi}{180} \quad \text{(Eq 4)}$$

Combining the Eshelby method (Ref 7) and the Mori-Tanaka concept of 'average stress' (Ref 8), for the two-phase composite materials with homogenous isotropic matrix and spheroidal inclusions, if we only consider the principal stresses and make $\varphi = 0$, the phase stresses can be separately determined: (Ref 9)

$$\left(\sigma_{11}^{M} - \sigma_{33}^{M}\right) = 3P\cdot\left(\sigma_{11}^{0} - \sigma_{33}^{0}\right) - 3B_1 f\cdot\left(\Delta\varepsilon_{11}^{P} - \Delta\varepsilon_{33}^{P}\right)$$

$$\text{(Eq 5)}$$

$$\left(\sigma_{11}^{I} - \sigma_{33}^{I}\right) = 3P^*\cdot\left(\sigma_{11}^{0} - \sigma_{33}^{0}\right) + 3B_1(1 - f)\cdot\left(\Delta\varepsilon_{11}^{P} - \Delta\varepsilon_{33}^{P}\right)$$

$$\text{(Eq 6)}$$

where, $\sigma_{11}^{M} - \sigma_{33}^{M}$ and $\sigma_{11}^{I} - \sigma_{33}^{I}$ refer to the stresses in the matrix and the inclusion, respectively; f is defined as the volume fraction of the inclusion; $\sigma_{11}^{0} - \sigma_{33}^{0}$ refers to the macroscopic stress; $\Delta\varepsilon_{11}^{P} - \Delta\varepsilon_{33}^{P}$ is the misfit of plastic strain between the matrix and the inclusion and can be given by:

$$\Delta\varepsilon_{11}^{P} - \Delta\varepsilon_{33}^{P} = \frac{P}{Q}\left(\sigma_{11}^{I} - \sigma_{33}^{I}\right) - \frac{P^*}{Q}\left(\sigma_{11}^{M} - \sigma_{33}^{M}\right) \quad \text{(Eq 7)}$$

The parameters stated above can be determined as follows,

$$P = \frac{\mu - \beta(\mu - \mu^*)}{3B}, \quad P^* = \frac{\mu^*}{3B}, \quad Q = B_1\{3P(1 - f) + 3P^* f\},$$
$$B_1 = \frac{2(\beta - 1)\mu\mu^*}{3B}, \quad \mu = \frac{E}{2(1 + \nu)}, \quad \mu^* = \frac{E^*}{2(1 + \nu^*)},$$
$$B = \mu - \{\beta - f(\beta - 1)\}(\mu - \mu^*), \quad \beta = \frac{2(4 - 5\nu)}{15(1 - \nu)}$$

$$\text{(Eq 8)}$$

E and E^* are Young's moduli, ν and ν^* are Poisson's ratios of the matrix and the inclusion, respectively.

Substituting Eq 4 in Eq 7, finally, the misfit of plastic strain between the matrix and the inclusion can be measured by x-ray as follows:

$$\Delta\varepsilon_{11}^{P} - \Delta\varepsilon_{33}^{P} = \frac{P}{Q}\cdot\left[-\frac{1}{S_2}\right]_{Ph}^{I}\cdot\left[\cot\theta_0\cdot\frac{\partial(2\theta_0)}{\partial(\sin^2\psi)}\cdot\frac{\pi}{180}\right]^{I}$$
$$- \frac{P^*}{Q}\cdot\left[-\frac{1}{S_2}\right]_{Ph}^{M}\cdot\left[\cot\theta_0\cdot\frac{\partial(2\theta_0)}{\partial(\sin^2\psi)}\cdot\frac{\pi}{180}\right]^{M}$$
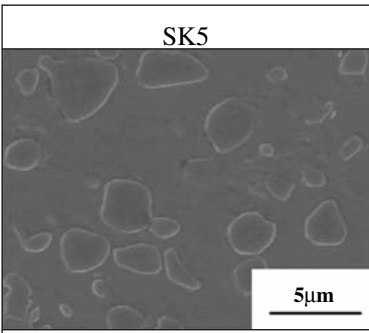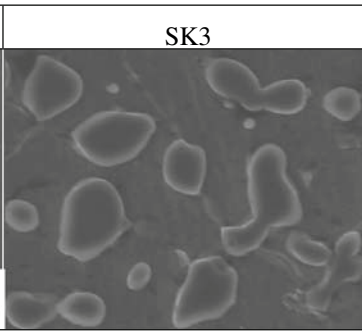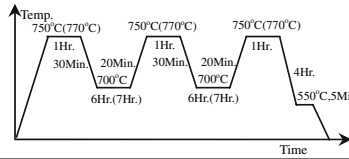
$$\text{(Eq 9)}$$

In Eq 9, the superscripts M and I mean the matrix and the inclusion, respectively; the subscript Ph means the material is in single phase state. For example, $\left[-\frac{1}{S_2}\right]_{Ph}^{I}$ means the x-ray elastic constant of the inclusion in single-phase state.

3. Experimental Procedure

3.1 Material and Specimen Preparation

Carbon steels JIS SK5 and SK3 are used in the experiment. The chemical composition is (mass percent,%): C 0.83(1.10),

Table 1 Micrographs, heat treatments and mechanical properties of the materials

SK5	SK3
$d = 2{\sim}3\,\mu m$	$d = 2{\sim}4\,\mu m$
$f = 13.1 \pm 0.1\,(\%)$	$f = 16.0 \pm 0.1\,(\%)$
$E = 189$ GPa, $\sigma_Y = 327$ MPa	$E = 183$ GPa, $\sigma_Y = 364$ MPa

d- Dimension of cementite particle, f - Volume fraction of cementite;
E - Mechanical Young's modulus; σ_Y - Yield stress.

Si 0.20(0.29), Mn 0.39(0.42), P 0.016(0.017), and S 0.005 (0.008). Spheroidal cementite particles that distributed throughout ferrite matrix are obtained by spheroidize annealing treatments. Heat-treatment procedure, micrographs, and mechanical properties of the materials after the heat treatments are listed in Table 1. Neither texture nor grain size distribution are observed in the materials. The specimen for tensile test used in present work is the same size, as that previously used, (Ref 10) which is with a gauge length 65 mm long and 3 mm square section. Geometry of the specimen for 4-point bending test is shown in Fig. 3. In order to realize stress measurement on the cementite phase by x-ray under the usual condition, surface treatment on the specimen is necessary (Ref 10). The treatment procedure is as follows:

1. Polish the oxidized and decarburized layers, about 0.1 mm in total depth, by emery papers.
2. Polish the surface electrochemically with a solution of 10% $HCLO_4$, 70% C_2H_5OH and 20% H_2O under 0.2 A direct current.
3. Wet polish the surface carefully with alumina powder, 0.5 mm in diameter.
4. Finally, corrode the surface slightly by a solution of 10% HNO_3, 60% CH_3OH and 30% of H_2O.

After the surface treatment, compressive residual stresses are observed in both phases. The residual stress is not more than 20 MPa in the ferrite and not more than 50 MPa in the cementite. These stresses are considered as the initial residual stresses in specimens.

3.2 Deformation Test and X-ray Stress Measurement

Stress state estimations for the ferrite and the cementite are performed in two experiments. In the first experiment, residual
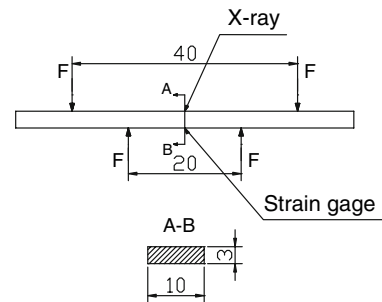
Fig. 3 Geometry of 4-point bending specimen

stresses are determined in each phase of specimens with 1, 2, 2.7, 4, and 7% of elongation, respectively. In these tests, the directions of stress measurement and deformation are the same ($\varphi = 0$). In the second experiment, internal stress distribution measurement in the *in situ* loading is performed using a 4-point bending fixture mounted on the sample holder of the diffractometer. In the two experiments, the elongations of specimens in the tensile test and the applied strains in the 4-point bending test are measured by strain gage.

In the stress measurements, the ferrite and cementite peaks are scanned with a scintillation detector at 30 kV and 10 mA (Rigaku MSF-3M). Stresses are measured with chromium radiation using 211 peak at approximately 156°2θ for the ferrite and 250 peak, 148°2θ for the cementite. The ferrite are scanned from 152° to 162°2θ at intervals of 0.1° per second and the cementite, from 145° to 151°2θ at intervals of 0.1° per 25 s a point. It lasts about three hours for the stress measurement of the cementite. Position of the diffraction peaks are determined by half-value breadth method for the ferrite, evaluated in terms of the center of Gaussian curve for the cementite data. In order

to estimate the stress states of each phase in the composite material precisely, it is necessary to determine the XEC of the material in the single-phase state (PXEC). However, because it is difficult to obtain the single-phase cementite bulk material, the PXEC of cementite that are directly measured by experimental ways have never been reported until now. In our previous study, (Ref 3) the XEC of the material in composite state (CXEC) for the ferrite and the cementite phases have been determined by a 4-point bending experiment, and the PXEC can be calculated using the relationship between the CXEC and the PXEC. The PXEC for the cementite are determined as $E_x = 269$ GPa, $v_x = 0.24$; and $E_x = 234$ GPa, $v_x = 0.29$ for the ferrite. In present work, the same PXEC values are used.
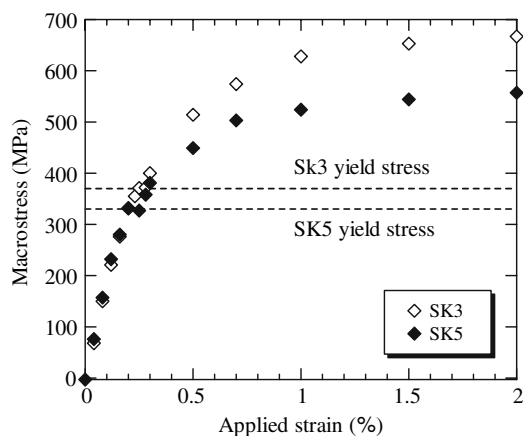
3.3 Optical Observations

In our study, scanning electron microscopy (Hitachi S-4500) is used as an assistance to observe the deformation behaviors of the cementite particles in the deformed steels. After the uniaxial tensile test, the specimen is polished by emery paper, about 1 mm in depth, and microstructure of the specimen inside is investigated.

4. Results and Discussion

4.1 Macroscopic Response Observed by X-ray

Figure 4 shows the macroscopic stress-strain curves of SK5 and SK3 that were recorded in the x-ray measurement acquisition of the *in situ* 4-point bending test. It indicates that SK5 and SK3 start to deform plastically after the applied strains exceed 0.28% and 0.32%, respectively. The Young's moduli E and yield stresses σ_Y decided from the stress-strain curves in the *in situ* 4-point bending test by x-ray (SK5: 183 GPa, 330 MPa; SK3: 179 GPa, 370 MPa) are similar to the data, which are decided from the strain gage recorded stress-strain curves in the tensile test, listed in Table 1. This means, within the x-ray penetration layer, the mechanical behaviors exhibited in the 4-point bending test are similar to those exhibited in the tensile test. Furthermore, it has been proved in our previous study that the residual stresses measured by x-ray in the tensile deformed specimens do not obviously deviate along the depth from the specimen surface (Ref 3). So, it suggests that the x-ray

measured stress states within the penetration layer reflect the bulk stress behaviors of the tensile deformed specimens.

4.2 Evolutions of Stress Under Loading and Residual Stress After Relaxation

Figure 5 shows that under the *in situ* 4-point bend loading, tensile stresses are observed in both phases and the stress states of the cementite are higher than those of the ferrite. After the uniaxially tensile tests, Fig. 6(a) shows that compressive residual stresses are observed in the ferrite as well as tensile ones in the cementite. It is also observed in the two figures that the stress states of SK5 are different from those of SK3: in the cementite, the stress in SK5 has greater magnitude than that in
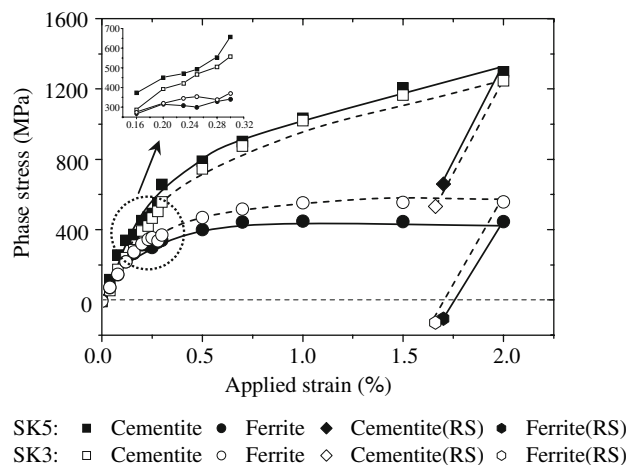
Fig. 5 Stress distributions in the *in situ* 4-point bending test
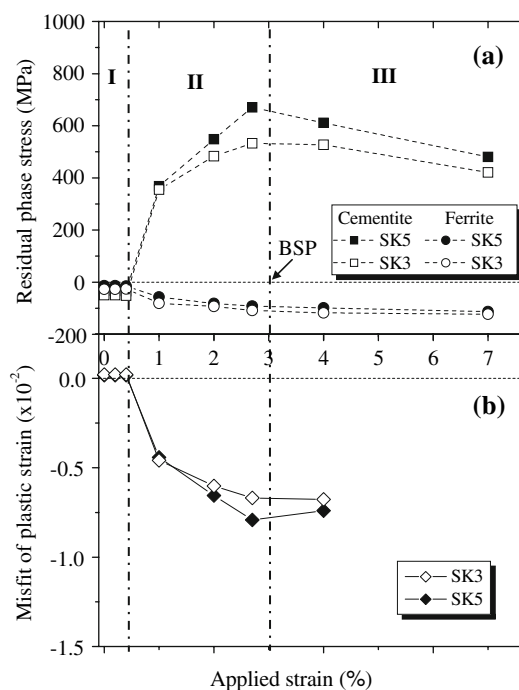
Fig. 6 Residual stresses and the misfit of plastic strain between the two phases in function of applied strain after the tensile deformation test

Fig. 4 X-ray measured macro stress-strain curves in the *in situ* 4-point bending test

SK3; in the ferrite, however, the stress in SK3 has greater magnitude than that in SK5. This means that the volume fraction of the cementite affects on the stress state of each phase not only under loading, but also after relaxation (Ref 3). In Fig. 6(b), the misfit of plastic strain between the cementite and the ferrite after tensile deformation is obtained by the residual stresses shown in Fig. 6(a) using the relationship described in Eq 7. The misfit of plastic strain between the ferrite and the cementite is only estimated up to applied strain of 4%. Since a good deal of broken cementite particles are observed on the specimen surface in the further more elongation, it does not satisfy the premise of the theoretical calculation on the misfit of plastic strain any more, that there is a complete contact between the matrix and the inclusion particle (Ref 9).

According to the evolution behaviors of residual stress in the cementite that shown in Fig. 6(a), we divide the whole stress evolution into three stages:

- In the first stage, except the initial residual stresses in the two phases, no residual stress generates in each phase, and the misfit of plastic strain between the two phases is about zero. The corresponding applied strain of this stage is until about 0.3%.
- In the second stage, residual stresses generate in both phases and the misfit of plastic strain between the two phases increases with the applied strain. This stage is from applied strain of 0.3% up to about 3%. It is noted that the residual stresses in the cementite cannot keep growing linearly in this stage, and the misfit of plastic strain shows the same evolution behavior.
- In the last stage, which starts from applied strain of 3%, the residual stresses in the cementite decrease slowly with the further strain after a stress saturation.

4.3 Characterization of the Deformability of Cementite from Residual Stress Evolution

In Stage I, except for the initial residual stresses in the two phases, no residual stress is generated in each phase, and the misfit of plastic strain between the two phases is about zero. This shows both the ferrite and the cementite to exhibit an elastic behavior in this stage.

In Stage II, residual stresses are generated in both phases, and the misfit of plastic strain between the two phases increases with the applied strain. This means at least one phase starts a plastic deformation in this stage. From the stress evolutions of the cementite and the ferrite shown in Fig. 5, we observe that the stress in the ferrite increases steadily with the applied strain until a point (it is about 0.2% for the SK5, and about 0.26% for the SK3), drops suddenly, and then rises with further strain. This point is the yield point of the ferrite and indicates the ferrite will begin to yield and deform plastically thereafter. In the cementite, however, the stress keeps an increase with the applied strain and no yield-point phenomenon is found. This indicates that the ferrite begins to deform plastically after entering Stage II.

It is observed in Stage II that the residual stress in the cementite cannot keep linear growth, and the misfit of plastic strain shows the same evolution behavior. Two reasons that may induce this phenomenon are considered. One reason is that the cementite begins a plastic deformation and induces a slowdown in the misfit of plastic-strain increase. This is

because if the cementite deforms elastically and the ferrite deforms plastically without relaxing, the misfit of plastic strain between the ferrite and the cementite will keep a linear increase with the applied strain. The other reason considered is that the cementite particles deform elastically and the ferrite deforms plastically, but a relaxation of plastic strain occurs in the ferrite with the increase of the applied strain. In this case, due to the obstruction of the matrix, the stresses in the cementite particles cannot relax to zero and are retained with residual stresses after unloading. Therefore, the plastic strain relaxation in the ferrite induces the residual stress in the cementite and the misfit of plastic strain between the two phases cannot keep linear growth.

As the relationships described in Eq 5 and Eq 6, the variations of $\sigma_{11}^I - \sigma_{33}^I$ and $\sigma_{11}^M - \sigma_{33}^M$ with $\Delta\varepsilon_{11}^P - \Delta\varepsilon_{33}^P$ can be represented as shown in Fig. 7. $\sigma_{11}^M - \sigma_{33}^M$ and $\sigma_{11}^I - \sigma_{33}^I$ refer respectively to the stresses in the ferrite and the cementite, $\Delta\varepsilon_{11}^P - \Delta\varepsilon_{33}^P$ refers to the misfit of plastic strain between the two phases, and σ_Y^M and σ_Y^I refer to the yield stresses of the ferrite and the cementite, respectively. After entering Stage II, it has been proven that the ferrite begins to deform plastically while the cementite, however, still deforms elastically. Thus $\sigma_{11}^M - \sigma_{33}^M > \sigma_Y^M$ and $\sigma_{11}^I - \sigma_{33}^I < \sigma_Y^I$. This means that $\Delta\varepsilon_{11}^P - \Delta\varepsilon_{33}^P$ is affected by the plastic strain in the ferrite and it increases while no plastic strain occurs in the cementite. With the increase of the applied strain, $\Delta\varepsilon_{11}^P - \Delta\varepsilon_{33}^P$ increases and achieves a certain value $\Delta\varepsilon_1^P$. Then the cementite begins to deform plastically, since $\sigma_{11}^I - \sigma_{33}^I = \sigma_Y^I$ is satisfied. However, an instant increase of plastic strain in the cementite induced by the start of plastic deformation will cause a decrease in $\Delta\varepsilon_{11}^P - \Delta\varepsilon_{33}^P$. The cementite and the ferrite thereafter will continue to deform keeping the misfit of plastic strain as much as $\Delta\varepsilon_1^P$. Therefore, to judge if the cementite begins to deform plastically in the Stage II, we have to investigate the evolution of $\Delta\varepsilon_{11}^P - \Delta\varepsilon_{33}^P$ during Stage II under the loading.

The misfit of plastic strain between the two phases and the full width of half maximal intensity (FWHM) of the two phases in the SK5 are investigated in the *in situ* 4-point bending test. As Fig. 8 shows, when the applied strain reaches ε_A, which is not more than 2%, the misfit of plastic strain between the two phases does not continue to grow linearly with the applied strain. In addition, Fig. 9 shows that FWHM of the ferrite phase does not continue to grow linearly and that of the cementite decreases simultaneously after the applied strain reaches ε_A.
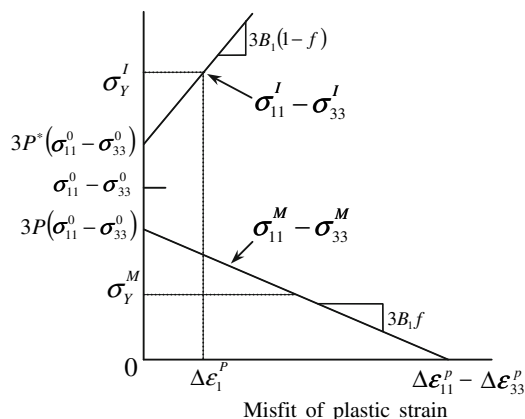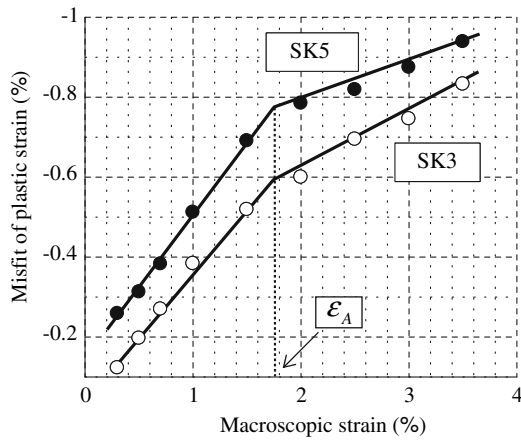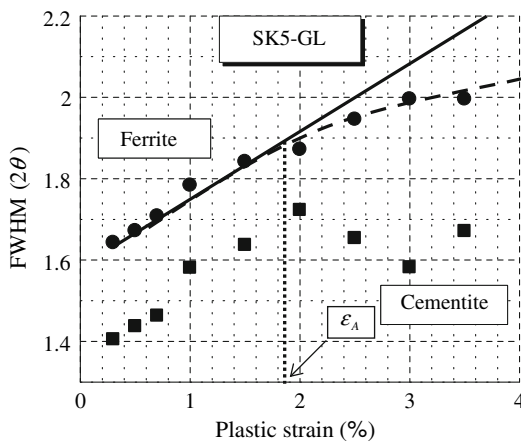

Fig. 7 Stress in each phase as a function of $\Delta\varepsilon_{11}^P - \Delta\varepsilon_{33}^P$ when the uniaxial stress is applied

Fig. 8 The misfit of plastic strain between the ferrite and the cementite in *in situ* 4-point bending test

Fig. 9 Peak width evolution in two phases in *in situ* 4-point bending test

However, ε_A should not be considered as the start strain point for the cementite plastic deformation, because the evolution behavior shown in Fig. 8 is different from the evolution behavior of $\Delta\varepsilon_{11}^P - \Delta\varepsilon_{33}^P$ expressed in Fig. 7, in which $\Delta\varepsilon_{11}^P - \Delta\varepsilon_{33}^P$ decreases if the cementite begins to deform plastically. Associating with the evolutions of the FWHM of the two phases shown in Fig. 9, it implies that there are other reasons induce a plastic relaxation in the ferrite before the cementite begins to deform plastically.

In a two-phase material, if the matrix deforms plastically and the particles deform elastically, then plastic shear of the matrix is accompanied by the build-up of elastic stresses in the neighborhood of the particles. In dislocation terms, the shear of the matrix will leave a loop of dislocation around every particle. These loops are named as "Orowan loops," and they act together to produce large stresses in the vicinity of the particles (Ref 11-14). As the Orowan loops accumulate round a particle, the pile-up may become unstable and will be modified by the following different ways: (i) the particle may shear; (ii) fracture may occur at the interface; (iii) the screw part of the loop may crossslip; (iv) the edge part of the innermost loop may climb. The (i) and (ii) break and relax the cementite particles, while (iii) and (iv) relax the ferrite matrix plastically.

Mechanisms of Orowan loops have been applied by Bate and Wilson on explaining the role of internal stresses that developed in the work hardening of spheroidised steels (Ref 15, 16). It is considered in present study that Orowan loops develop around the cementite particles and induce internal stresses in the deformed specimens. After unloading, due to the obstruction of the ferrite, the stresses in the cementite particles cannot relax to zero, and retained residual stresses as shown in Fig. 6(a). In the *in situ* 4-point bending test, Fig. 8 and 9 show the misfit of plastic strain between the two phases and that the FWHM of the ferrite cannot continue to grow linearly after the applied strain reaches ε_A. It indicates that while the applied strain reaches ε_A, the piled up Orowan loops make the stress around the cementite particle reach the theoretical shear stress of the ferrite or the cementite. The loops become unstable and may relax either by ways of (i) to (iv). (Ref 11) Figure 9 shows that the relaxations also induce a FWHM decrease in the cementite. However, few cementite particles that break in the ways of (i) and (ii) are found in the optical observation on the inside of specimens. These results indicate that, in the Stage II, the plastic strain relaxation occurs mainly in the ways of (iii) and (iv), and induces the residual stress in the cementite that cannot continue to grow linearly with the applied strain after the applied strain exceeds a certain strain value ε_A. For the materials used in the present work, ε_A is observed to be no more than 2%.

After the applied strain achieves a certain value, Fig. 6(a) shows that the residual stress in the cementite almost cannot increase with the applied strain any more. This means that the residual stress in the cementite has saturated. The residual stress saturation phenomenon has also been reported in other studies. Belassel et al. (Ref 17, 18) measured the residual stress in the cementite by synchrotron radiation (S.R). They found the residual stress in the cementite increased with the applied strain up to 3%, and decreased, thereafter. They attributed this phenomenon to the fracture of cementite particles. Oliver et al. (Ref 19) measured the residual stresses in spheroidized steels using neutron diffraction. They also reported that there was an initially high rate of change of residual strain in the cementite with plastic strain, but the saturation occurred after a few plastic strains. However, no decrease was observed in the residual strain evolution of the cementite up to plastic strain of 8%. In our study, to clearly express this phenomenon and correlate it with the deformation behaviors of the two phases, this corresponding applied strain value is named as the border strain point (BSP) in present study. The Stage III is defined from the applied strain achieves the BSP. It is difficult to find a certain strain point as the BSP that fits both the SK5 and the SK3 in this figure, so that we assume the BSP occurs at the applied strain of 3%.

Figure 6(a) shows that the residual stress in the cementite decreases slowly with the subsequent strain after entering the Stage III. A considerable reason that induces this phenomenon is that the cementite particles break in the ways of (i) and (ii) after entering Stage III, and the residual stresses are relaxed. This is because it has been proven in the previous studies that cementite particles in high-deformed steels will break in two ways: one is a crack separation at the boundary between the particle and the matrix; the other is a crack in the cementite particle (Ref 20-22). In present study, scanning electron microscopy is used to investigate the break ways of the cementite particles inside the specimens after the tensile deformation test. Figure 10 shows micrographs of the cementite particles that break in three ways: (a) a crack separation at
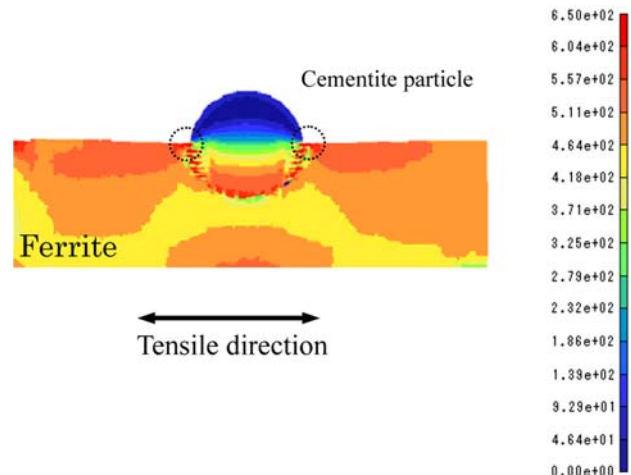
the boundary between the cementite particle and the ferrite; (b) a crack between two closely spaced cementite particles; (c) a crack in the cementite particle. For these types of cracks, it is suggested that the crack separation at the boundary between the cementite particle and the ferrite occurs previous to the particle crack, because the interface between the ferrite and the cementite breaks before the loading stress exceeds the high fracture strength of cementite at room temperature (420-840 kg/mm^2) (Ref 23). Goldenberg et al. (Ref 20) have demonstrated in their study that the void nucleation and growth occurs predominantly at a relatively weak interface and between two closely spaced carbide particles. In our observations, Fig. 10(c) indicates that the particle cracks are predominantly found in the elliptical cementite particles that are located on the grain boundary of the ferrite. This observation agrees well with the computational result of Sakamak et al. that the particle shape decides the position of stress concentration, and a particle crack usually occurs in the cementite particle with large axial ratio (i.e. the long-axis direction of particle is parallel to the tensile loading) (Ref 21). The crack occurring in this state of cementite particle is caused by the combination of a tensile stress transmitted from the applied stress, bending stresses transferred from two moments of flexion and a high shear stress caused by the dislocations piled up at the interface (Ref 22). We, therefore, conclude: after the shear stress caused by the Orowan loops reaches the theoretical yield strength of the ferrite, the cases (iii) and (iv) occur; if the shear stress reaches the fracture stress at the interface between the cmenenite particle and the ferrite, the case (ii) occurs; the case (i) only occurs in the cementite particle with large axial ratio, but it is caused by the combination of several forces, not only the shear stress induced by the Orowan loops.

In our study, we observed that the quantity of the broken particles inside the specimen increases with the increase of applied plastic strains, but the broken particles occupy only a little part, less than 3%, of all observed cementite particles in the specimen with an elongation of 7%. Figure 11 shows the micrograph of the specimen surface before the tensile deformation test. The micrograph shows that, after the surface treatment, the upside part of many cementite particles are emerged from the ferrite. We build a model that describes the cross section of this state cementite particles and simulate the stress distributions in the particle and the surrounding ferrite under the tensile stress. Figure 12 shows the simulation result of the model under a uniaxial tensile stress of 500 MPa. It indicates that the highest tensile stress concentrates at the boundary between the cementite particle and the ferrite near the specimen's surface. This stress concentration may induce
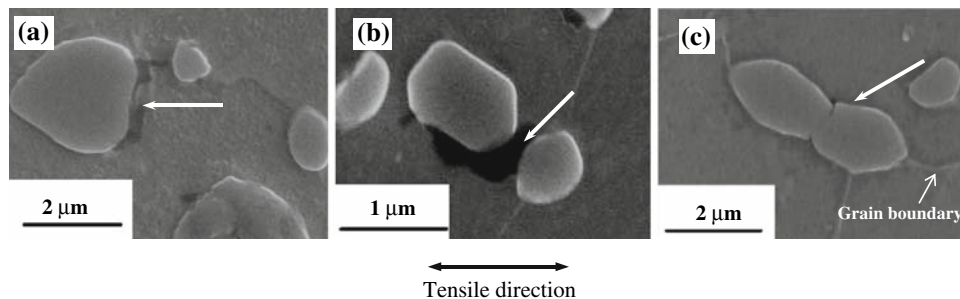
the crack separation at the boundary between the cementite particle and the ferrite. The optical observation on the surface of the tensile deformed specimen shown in Fig. 13 proves this result. After entering Stage III, we observe that the quantity of the cracked cementite particles on the specimen's surface increases sharply. On the surface of the specimen with an elongation of 7%, more than 30% of the observed cementite particles are broken. Considering x-ray measured stress in the cementite is representative of average stresses within individual irradiated cementite particles, we propose that the cracked
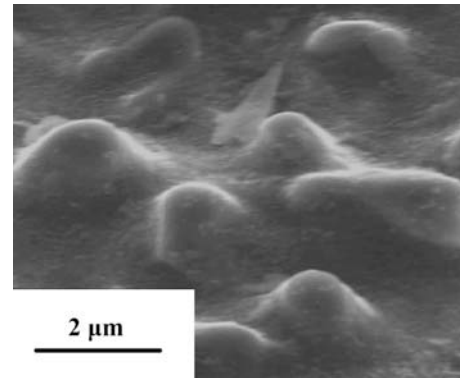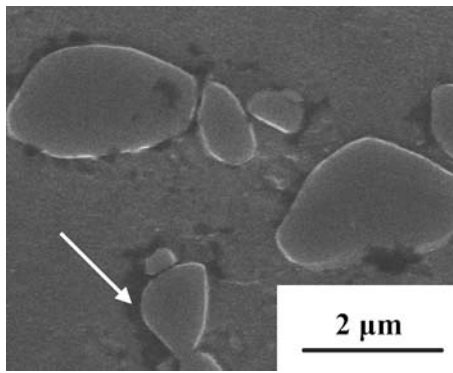

Fig. 11 Micrograph of the specimen's surface before the tensile deformation test

Fig. 12 Simulation of the stress distributions in the cementite particle and the surrounding ferrite (in cross section) under the tensile stress of 500 MPa

Fig. 10 Crack in particle and at boundary, (a) Crack separation at interface, (b) Crack between two cementite particles, and (c) Crack in cementite particle

Fig. 13 Micrograph of the specimen's surface after the tensile deformation test

cementite particles on the specimen's surface induce a stress decrease after entering Stage III. This proposition simply explains why no decrease was observed in the residual strain evolution of the cementite up to plastic strain of 8% in the study of Oliver et al. (Ref 19) Due to the greater penetration depth of neutron diffraction ($\sim$10 mm for iron, compared to $\sim$ 10μm for x-rays of comparable wavelength), the influence of the stress relaxation induced in the cracked cementite particles on the specimen's surface is so slight that it can be ignored.

From the discussions above, we conclude the evolution behaviors of the residual stress shown in Fig. 6 to be as follows: in Stage I, except the initial residual stresses in the two phases, no residual stress is generated in each phase; in Stage II, the ferrite begins to deform plastically, and relaxation occurs in the ferrite at the following applied strain making the residual stress in the cementite unable to increase linearly and saturate thereafter; in Stage III, the broken cementite particles on the specimen's surface induce a residual stress decrease in the cementite. For the cementite, the discussions indicate that the spheroidal cementite particle has no plastic activity, yet, even though the BSP occurs. In the following deformations, we consider that the cementite particle breaks within its elastic limit, because the brittleness of cementite has been well recognized in the previous studies: tensile deformation of the thick cementite lamella in pearlite favors brittle failure; (Ref 2) the polycrystalline bulk cementite is brittle and fractures within its elastic limit when deformed below 573 K (Ref 6). In summary, the different deformation steps that have been characterized from the residual stress state evolutions are:

- A first step where the ferrite and the cementite have an elastic behavior;
- A second step, in which the cementite is still elastic and the ferrite is plastic;
- A third step where plastic strain relaxation occurs in the ferrite but cementite still deforms elastically;
- Finally, the cementite breaks.

5. Conclusion

X-ray diffraction technique has been applied successfully to estimate the stress state evolutions for the ferrite and the cementite in the deformed spheroidized carbon steels. In the *in situ* 4-point bending test, both the cementite and the ferrite show the tensile stresses, and the stresses increase with the

applied strain. After the uniaxial tensile test, the ferrite shows the compressive residual stress, and the cementite shows a tensile one. It is observed that the residual stress in the cementite saturates after achieving a certain applied strain and decreases thereafter. We name this applied-strain value as the border strain point (BSP) and prove that it is in induced by the relaxation that occurr in the ferrite. The cracked cementite particles on the specimen's surface induce a residual stress decrease in the cementite.

The coupling of x-ray diffraction and optical observations allows for the linking of the stress state to the mechanical behaviors of each phase. It permits a characterization of the deformability of the spheroidal cementite particle in the carbon steel using residual stress measurement. The results indicate the cementite particles in spheroidized carbon steel show an elastic behavior in the whole deformation processing until it breaks.

References

1. J.D. Embury and R.M. Fisher, The Structure and Properties of Drawn Pearlite, *Acta Met.*, 1966, **14**, p 147–159
2. G. Langford, Deformation of Pearlite, *Met. Tran.*, 1977, **8A**, p 861–875
3. L. Che, M. Gotoh, M. Horimoto, and Y. Hirose, Effect of Microstructure of Cementite on Inter-phase Stress State in Carbon Steel, *J. Iron. Steel. Res. Int.*, 2007, **14**(4), p 31–38
4. D.A. Porter, K.E. Eastering, and G.D.W. Smith, Dynamic Studies of The Tensile Deformation and Fracture of Pearlite, *Acta Met.*, 1978, **26**, p 1405–1422
5. M.H. Hong and W.T. Reynolds, Jr., et al., Atom Probe and Transmission Electron Microscopy Investigations of Heavily Drawn Pearlitic Steel Wire, *Met. Mater. Trans.*, 1999, **30A**, p 717–727
6. M. Umemoto, Y. Todaka, and K. Ysuchiya, Mechanical Properties of Cementite and Fabrication of Artificial Pearlite, *Mat. Sci. Forum*, 2003, **426–432**, p 859–864
7. J.D. Eshelby, The Determination of the Elastic Field of an Ellipsoidal Inclusion, and Related Problems, *Proc. R. Soc. London*, 1957, **241A**, p 376–396
8. T. Mori and K. Tanaka, Average Stress in Matrix and Average Energy of Materials with Misfitting Inclusions, *Acta Met.*, 1973, **21**, p 571–574
9. T. Sasaki, Z. Lin, and Y. Hirose, X-ray Measurement of Plastic Strain by Means of Eshelby/Mori-Tanaka Model and Its Application, *Jpn. Soc. Mech. Eng.*, 1997, **63A**, p 158–165 In Japnese
10. L. Che, M. Gotoh, Y. Horimoto, and Y. Hirose, X-ray Stress Estimation of Carbide Spheroidized JIS SK5 Steel, *Mat. Sci. For.*, 2006, **524–525**, p 943–948
11. P.M. Hazzledine and P.B. Hirsch, A Coplanar Orowan Loops Model for Dispersion Hardening, *Phil. Mag.*, 1974, **3**, p 1331–1351
12. L.M. Brown and W.M. Stobbs, The Work-hardening of Copper-Silica: I. A Model Based on Internal Stresses, with no Plastic Relaxation, *Phil. Mag.*, 1971, **23**, p 1185–1199
13. L.M. Brown and W.M. Stobbs, The Work-hardening of Copper-Silica: II. The Role of Plastic Relaxation, *Phil. Mag.*, 1971, **23**, p 1201–1233
14. J.D. Atkinson, L.M. Brown, and W.M. Stobbs, The Work-hardening of Copper-Silica: IV. The Bauschinger Effect, *Phil. Mag.*, 1974, **30**, p 1247–1280
15. P.S. Bate and D.V. Wilson, Analysis of the Bauschinger Effect, *Acta Metall.*, 1986, **34**(6), p 1097–1105
16. D.V. Wilson and P.S. Bate, Reversibility in the Work Hardening of Spheroidised Steels, *Acta Metall.*, 1986, **34**(6), p 1107–1120
17. M. Belassel, J.L. Lebrun, and S. Deis, et al., Effect of Thermal and Mechanical Loading on the Generation of Macro and Micro Stresses in Eutectoid Steel, *4th Inter. Conf. on Residual Stress (ICRS4)*, Authorhouse, Baltimore, 1994, p 392–401
18. M. Belassel, V. Ji, and J.L. Lebrun, et al., Analysis of the Mechanical Behavior of Materials Through the 2nd and 3rd Order Stress, *J. De Physique IV*, 1994, **C9**, p 261–264
19. E.C. Oliver, M.R. Daymond, and P.J. Withers, Interphase and Integranular Stress Generation in Carbon Steels, *Acta Mater.*, 2004, **52**, p 1937–1951

20. T. Goldenberg, T.D. Lee, and J.P. Hirth, Ductile Fracture of U-Notched Bend Specimens of Spheroidized AISI 1095 Steel, *Met. Tran.*, 1978, **9A**, p 1663–1671

21. K. Sakamaki, S. Inada, and S. Hori, Tensile Fracture of Spheroidized 0.7% Carbon Steel at Low Temperature, *J. Soc. Mat. Sci. Jpn.*, 1981, **30**, p 49–55 in Japanese

22. M. Hamada, K. Sakamaki, and S. Inada, The Role of Cementite on the Fracture of Spheroidized Cementite Steel (In the case of the cementite particle existing in ferrite grain), *Eng. Data. Uni. Tokushima.*, 1983, **28**, p 11–19 in Japanese

23. W.W. Webb and W.D. Forgeng, Mechanical Behavior of Microcrystals, *Acta Met.*, 1958, **6**, p 462–469